Probing instabilities in arc plasma devices using binary gas mixtures

S. Ghorui, M. Vysohlid, J. V. R. Heberlein, and E. Pfender
Department of Mechanical Engineering, University of Minnesota, Minneapolis, Minnesota 55455, USA
(Received 23 March 2007; published 19 July 2007)

This paper presents an experimental approach to identify the sources of instabilities in arc plasma devices. The phenomena of demixing in arcs have been utilized to explore the characteristics of different instabilities. Problems in explaining the observed behavior with our current understanding of the phenomena are discussed. Hydrogen is used as a secondary gas with argon as the primary plasma gas for this study. Results indicate that the observed behavior such as steady, takeover, and restrike modes of instabilities in arcs may essentially originate from the thin boundary layer over the anode wall primarily at the location of the anodic arc root. The bulk core flow apparently does not play any significant role in such instabilities. Arc currents rather than flow rates control the behavior of the instabilities in frequency space. Bifurcation of the system behavior and evidence for the existence of quadratic zones in flow space of binary gas mixtures separating steady and unsteady behavior are discussed.

DOI: 10.1103/PhysRevE.76.016404 PACS number(s): 52.75.Hn, 52.70.−m, 81.15.Rs

I. INTRODUCTION

An arc plasma device is a hardware designed to convert electrical energy of the arc to thermal energy of the plasma jet. It is a complex system having large number of influencing parameters and exhibits a vast variety of dynamical behavior. The physical and operational state of an arc plasma system is best described in terms of its static and dynamic characteristics. Static characteristics normally indicate the steady state behavior whereas dynamic characteristics describe the evolution of the system behavior with time. Instabilities arising out of interaction among electromagnetic, fluid dynamic and thermal fields inside such devices give rise to nonlinear time evolution of associated plasma quantities. Manifestation of the symptomatic behavior in electric arcs through various arc modes owing to these instabilities is a complicated but important phenomenon that remained as a subject of active research over the past four decades [1–14] and it is a continuing concern for numerous technical applications. The challenge is to understand the origin of such instabilities, predict the regimes of stable/unstable operations, determine control parameters for excitation of these instabilities and validate the hypotheses through experiments. The objective of this paper is to discuss the fundamental problems associated with the dynamics based on recent experimental investigations and theoretical developments and to introduce an experimental approach for probing the dynamics of such arcs. The latter may have the potential of exploring the arc dynamics in more detail than previous approaches.

The symptomatic behavior of arcs, found in many arc devices, depends primarily on the particular operating conditions and the plasma gas used. It can be characterized in terms of three broadly classified modes [3]: steady, takeover, and restrike. Based on the observations through high-speed photography, spectroscopic temperature measurement, and calorimetric analysis, the specific anode attachments in different modes and the associated heat fluxes have been measured [3]. Phenomenological models of the observed behavior have been proposed [4] and an extensive investigation of the anode attachment instability using planar double anode has been reported [4] including the instability of the anode attachment under the influence of an impinging jet with laterally forcing gas [13,14]. In the latter case, a gradual increase of the lateral gas flow rate produced a restriking behavior for flow rates above a certain threshold. A detailed characterization of the behavior in terms of arc voltage fluctuations has been reported [5] for the restrike mode of operation. Studies have been reported on boundary layer thickness and associated arc instabilities in a plasma spray torch [7] and on anodic arc root behavior through time resolved imaging [8]. Arc voltage fluctuations in commercial plasma spray torches have been investigated in [9]. Following standard recipes of instability theory, such phenomena have been studied in [10–12] and comparisons with experimental results have been provided. Further theoretical developments and innovative experimental approaches are still necessary for a complete understanding of the actual mechanisms governing the observed arc behavior. A more detailed discussion on this is presented in the next section.

Space selective probing of the zones inside an arc plasma torch without disturbing the system is probably the best way to extract information on arc instabilities and thereby validate the postulated mechanisms driving such behavior. However, extremely high temperatures and inaccessibility to direct observation make this task extremely difficult. The present study introduces an approach to probe the instabilities in the inaccessible inner regions of the torches using a binary gas mixture as a plasma gas. The technique primarily rests on a process known as demixing [15–22] in arcs. Once a binary gas mixture enters the constricted plasma column, the demixing process drives spatial variations for each of the constituent gases depending on the diffusion coefficients and the existing temperature field. By varying concentrations of the constituent gases, desired spatial variations of the plasma composition are feasible, allowing the spatial probing of the associated zones. Detailed information on the composition of different zones inside the torch may be obtained through appropriate numerical simulation. In Sec. III we describe a two-temperature one-dimensional model (Elenbaas-Heller) [23] of the arc for deriving temperature profiles computed

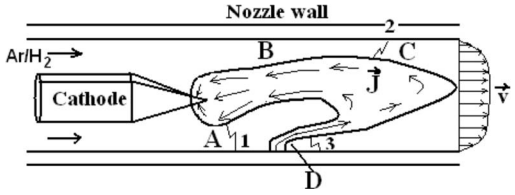

FIG. 1. Possible current path between the cathode and the nozzle. 1,2,3 are representative restrike points. The arc is divided into four zones: (A) Near cathode zone; (B) constricted zone adjacent to zone (A); (C) plasma loop; (D) zone near the arc root. "v" is the velocity profile; "J" is the current density.

with approximate velocity profiles, consistent with experiments, to obtain a qualitative estimate of the trend of the demixing behavior in an argon-hydrogen arc. It should be emphasized that the ultimate demixing behavior is highly dependent on the mole fraction and the degree of thermal nonequilibrium prevailing in the system [24]. In subsequent sections, we show that the idea of exploiting demixing behavior for spatial probing can confirm experimentally observed results and, in addition, it allows to extract a number of important pieces of information about the observed instability. A judicious mix of such experiments with appropriate numerical simulations will improve our understanding of arc instabilities.

II. SYMPTOMATIC BEHAVIOR IN ARCS AND THE PHENOMENA OF DEMIXING

For an understanding of the various forces acting on an arc, a possible layout of the current path between the cathode and the nozzle inside a typical plasma torch is sketched in Fig. 1, based on the observations through high-speed photographs [4]. Although a continuous optically bright zone in the photographs is likely to represent the path of the arc current, a current carrying zone may appear optically dark if the current distribution is more diffuse at the instant of the photograph. Since the cathode and anode are conductors and electric fields are always normal to a conducting surface, the current enters normally into both cathode and anode as shown in Fig. 1. The gas along the path of the arc current is heated to form a plasma and the plasma channel is subjected to the drag force exerted by the surrounding flow of cold gas. A thermal pinch near the anode is likely to produce an anode jet. The interaction with the main flow and this anodic jet, the cooling by the surrounding cold gas and the ohmic heating along the current carrying path results in the observed shape of the plasma loop. A cylindrical current channel segment of radius "r", radius of curvature "R", existing at a distance "l" from the cathode along the curved arc path in an ambient cold gas flow of velocity "v" is subjected to the following forces per unit length [4,6]:

electromagnetic body force:

$$F_B = -\frac{3\mu_0 I^2}{16\pi R(l)}\left[1 - \frac{7}{18}\left(\frac{r(l)}{R(l)}\right)^2\right], \quad (1)$$

gas dynamic drag force: $F_D = C_D r(l)\rho(l)v(l)^2$, (2)

Lorentz force due to external field: $F_L = I \times B_{ex}(l)$, (3)

where I is the total current, ρ is the mass density, and μ_0 is the permeability. C_D is the drag coefficient ($\sim$0.2 [4]), which is a function of the Reynolds number and heat transfer to the surrounding cold gas. B_{ex}, the magnetic field at the location "l," is composed of the magnetic induction derived from different sections of the current path. It must be emphasized that the self magnetic field produced by the current in the cathodic arc column may influence the resultant magnetic field (B_{ex}) experienced by the arc column near the anode attachment [6]. While F_B corresponds to the net force experienced by a curved arc column due to asymmetric interaction between arc current and self magnetic field, F_L accounts for the forces due to magnetic fields from other section of the arc [6].

All of the above three forces are highly space dependent and for a typical plasma torch configuration F_B acts in the direction opposite to that of F_D. It also may be noted that a change in any one of these forces eventually leads to changes in the other two. It has been shown in [4] that under typical operating condition, F_D and F_B may balance each other and the Lorentz force F_L may contribute to distorting the current path in a specific manner [6]. An interesting point to note is that both F_D and F_B vanish at the anode wall as R reaches infinity (the current enters normally into the conducting surface) and v becomes zero (no slip condition at the wall). This implies that such balances are meaningful only at the locations somewhat away from the arc root and not exactly at the anode wall. When an arc operates in the steady mode, the subtle balance of all these forces is perfectly maintained in all sections of the arc channel and a stationary configuration of the arc is observed. In the restrike mode, it is proposed [4] that F_D is stronger than F_B near the arc root and the resultant force drives the arc root downstream leading to a monotonic increase of the electric field that is experienced throughout the boundary layer. The arc root movement continues until the electric field becomes high enough to cause a breakdown of the boundary layer at some favorable upstream location forming a new arc root. The phenomenon repeats with time and the usual sawtooth arc voltage is observed.

While it has been realized that the hydrodynamic boundary layers adjacent to each anode may play a significant role in the arc dynamics [4], results of recent studies also indicate that there may be other reasons besides the above mentioned forces responsible for the control of the behavior of an arc. For example, in the takeover mode, which is characterized by a more diffuse anode arc root, there may or may not be a new arc root formation and erratic voltage fluctuations may occur through movement of the same arc root, there is no simple explanation for the kind of behavior observed. It is now well established that the flow inside a plasma torch is essentially laminar [25], and usually arcs have no memory of previous conditions [26]. Therefore, if the externally imposed operating conditions are not changed, the thickness as well as other properties of the upstream boundary layer are not likely to change appreciably owing to past breakdown, and hence the required electric field for breakdown will always be nearly the same. This should result in nearly iden-

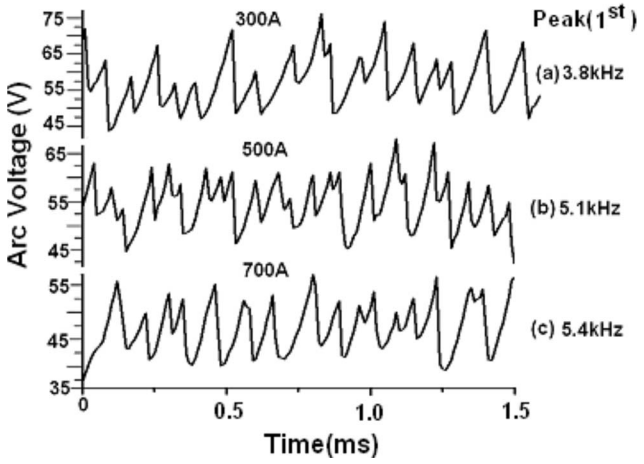

FIG. 2. An example of packing more waveforms into a given time interval with increase in current. Argon: 70 slm; hydrogen: 5 slm.

tical voltage minima and maxima as the restrike proceeds. Time evolution of arc voltage as obtained from 3D-CFD simulation in [26] implementing this restrike model, indeed reflects this assumption. However, in the experiment [26], the voltage minima are found to vary by more than 200%. Moreover, the primary restrike frequency obtained from the model turns out to be twice that of the experimental one and the simulated spectrum exhibits sharp peaks instead of the experimentally observed broadband behavior. An attempt to match the frequency by artificially increasing the local electric field strength results in unrealistic voltage jumps and velocity fields [26]. It also remains to be explained why the arc dynamics is so unpredictable as observed in numerous experimental studies. In [4] as the gas flow rate was increased to 170 m/s, where a transition to the restrike mode was expected, a high-frequency, irregular sinusoidal voltage fluctuation appeared instead. For $I>100$ A, only erratic voltage fluctuations were observed. As shown in [14], an increase in lateral gas flow rate (LGF) from 39 slm (standard liter per minute) to 42 slm in steps of 1 slm, the restrike frequency showed a decrease by some arbitrary amount in every step. Interestingly, as the LGF increased from 42 to 43 slm, the restrike frequency suddenly jumped up by more than 33%. For LGF=44 slm the frequency again came down by a substantial amount. Another interesting aspect that may be examined from various waveforms presented in this paper as well as from other similar studies is that over a wide range of operating conditions an increase in current simply packs a larger number of waveforms into a given time interval without changing the general features of individual waveforms in the time series. Time series, captured for 1.5 millisecond under three different arc currents (300, 500 and 700 A), exhibit this feature clearly in Fig. 2.

It is interesting to note that most of the features described above may be explained as a natural consequence in the study of instabilities in [10–12]. Here, the observed instability (by fluid dynamic flow fields and electromagnetic forces) in the zone near the arc root is analyzed in terms of an amplitude equation, following standard recipes of instability description. It is hypothesized that the balance of the forces

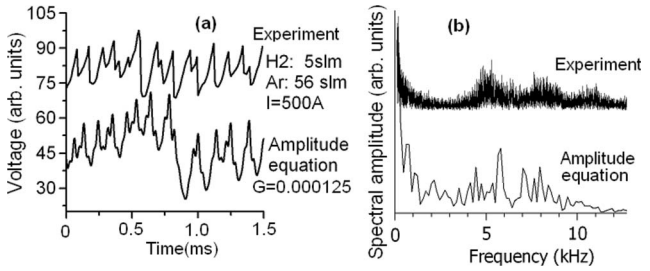

FIG. 3. Comparison of the time series obtained from experiment with that obtained from amplitude equation: (a) Time series; (b) frequency spectra of signals in (a).

[Eq. (1)–(3)] is subjected to the disturbances caused by this instability that occurs near the arc root, resulting in the kind of time behavior observed. Depending on the operating condition, the resulting instability in the electric field may lead to situations when breakdown at some upstream location(s) is energetically favorable and physical restriking of the arcs may take place. Otherwise, the oscillation may continue without restrike as observed in the takeover modes or it may vanish with time, leading to a steady mode. The amplitude of the instability (F) is obtainable in terms of dimensionless time from the amplitude equation [11]:

$$\dddot{F} + \mu_2 \ddot{F} + \mu_1 \dot{F} + \mu_0 = -F^3. \tag{4}$$

The behavior under the restrike mode is reproducible with $\mu_0=140$, $\mu_1=50$, and $\mu_2=1$. Real time "t" is recoverable from the dimensionless time "s" through the relationship:

$$t = G \cdot s, \tag{5}$$

where G is a parameter that depends on thermo-physical properties of the instability originating zone [12] and has an inverse relationship with the temperature. An increase in temperature results in a decrease in G, which in turn increases the frequency of the instability according to Eq. (5). Lower values of μ_0 are capable of reproducing various other oscillatory behavior observed under the broad category of takeover modes. The time series offered by Eq. (4) is actually chaotic, and hence never repeats; It adheres to seemingly unpredictable behavior (as experimentally observed) with time but remains bounded within some zone (called attractor) in the physical domain. The broadband feature of experimental signals also happens to be an inherent characteristic of chaotic time series. Equation (4) also incorporates catastrophic behavior for certain coefficient values where the solution becomes suddenly unbounded. Remarkable similarities between experimental waveforms of arcs and those generated using the amplitude equation are presented in [12] over a wide range of experimental conditions. Similar comparisons for the typical experimental signals encountered in this study are presented in Fig. 3(a) for a time series and in Fig. 3(b) for corresponding frequency spectra. Overall similarities between experimental and theoretical behavior are reasonable.

Thus, an explanation of the observed symptomatic behavior is obtainable in terms of the amplitude equation of instability. At least, this equation is capable of explaining all the

observed behavior (steady, take over, restrike, and sudden extinction) from a single theory. However, it is based on the hypothesis that the instability originates from the zone near the anodic arc root (zone "D" in Fig. 1) and compares the resulting instability with the measurements of the dynamic arc voltage that evolves as

$$V_{\mathrm{arc}}(t) = \int_{l=0:\mathrm{nozzle}}^{l=L:\mathrm{cathode}} I\Re(l,t)dl, \tag{6}$$

where the integration is carried out along the curved path of the arc channel from the nozzle to the cathode and $\Re(l,t)$ is the time varying resistance per unit length of the arc at the location "l" of the path. While, $\Re(l,t)$ is expected to have a complicated dependence on path, its variations in any of the zones, like "A" , "B", "C" or "D" (Fig. 1) is capable of inducing a variation in V_{arc}. Moreover, the aerodynamic drag force is highest in the zone "C" as it is exposed to the peak of the velocity profile. Therefore, for a complete understanding it is necessary to know the exact contributions of the core *vis-à-vis* that of the boundary layer on these instabilities. Also, the arc current as well as the gas flow field has the potential to influence $\Re(l,t)$. It is necessary to identify the specific contribution of each of them on the instability behavior. Forces in Eqs. (1)–(3) as well as the "G" factor in Eq. (5) are all dependent on thermophysical properties of the instability-originating zone. To be certain about the origin of these instabilities it is necessary to experimentally verify the functional relationships of these parameters with the thermophysical properties resulting from corresponding theories.

Demixing of binary gases in the temperature field of an arc offers a natural way to vary composition of different regions inside an arc device (plasma torch) through variation of inlet flow conditions of individual gases. Associated changes in the instability features may reveal important information about the spatial location of the origin of such instabilities as well as its parametric dependence on plasma conditions. In most of the arc plasma torches, plasma columns exist with almost radially symmetric temperature profiles, having a high temperature peak at the center and nearly ambient temperature at the wall. It has long been known [15] that even if a uniformly mixed binary gas mixture is introduced in such arcs, demixing processes can cause radially symmetric separation of the component gases once they enter the arc column leading to observations like "Lenard's hollow flame" in arcs [15]. Recently, Murphy [17–20], Murphy and Hiraoka [21], Murphy and Snyder [22] have made extensive theoretical and experimental investigations of such processes. It has been observed that partial pressure gradients, frictional forces, thermal diffusion and external forces [19] are responsible for such demixing phenomena. A particular spatial demixing behavior depends on specific components of the plasma gas used, their diffusion coefficients as well as on the temperature profile inherited by the arc column owing to the particular design of the torch and the prevailing operating conditions. The larger the difference in the masses of the component gas molecules, the larger the effect of demixing. It has been reliably observed experimentally [22] in a free burning argon-hydrogen transferred arc upon changing concentrations of hydrogen in argon, that the relative concentrations of hydrogen at and around 5 mm from the axis remained nearly unchanged but significant changes for $r>5$ mm occurred. Due to experimental limitations, it was not possible to observe the behavior in the region around the central axis (at radii much less than 5 mm). It has also been concluded in their study [22] that non-LCE (local chemical equilibrium) effects may lead to an additional increase in hydrogen concentration at the periphery. It is expected that the existence of sharper gradients inside the constrictor nozzle of nontransferred arc torches will enhance the effect further near the water-cooled anode wall. However, the demixing phenomenon is highly sensitive to the existing temperature field and it should be mentioned that Murphy and Hiraoka [21] observed an increase in hydrogen concentration in the center of a free-burning arc, at temperatures about 15 000 K.

The idea of using binary gas mixtures for instability studies originates from the results of the above studies. Owing to the large mass difference between argon and hydrogen, this combination is chosen in this experiment to realize a pronounced effect of the phenomenon. Small changes in the hydrogen flow rate in the feeding line may not significantly influence the core region of the arc, but may appreciably influence the boundary layer. By varying concentrations of hydrogen and noting corresponding changes in instability behavior, it may be possible to determine if the instability originates in the boundary layer in front of the anode.

Inside arc plasma torches, both chemical and thermal nonequilibria exist and conservation of the number density (n_k) of species "k" can be written as [27]

$$\frac{\partial n_k}{\partial t} + \vec{\nabla}\cdot(n_k\vec{u}) + \vec{\nabla}\cdot\vec{g}_k = \dot{n}_k. \tag{7}$$

$n_k\vec{u}$ is the convective flux and $\vec{g}_k$ is the diffusive flux of species "k". $\vec{u}$ is the velocity vector and t is time. Neglecting the influence of external forces [19], the diffusive flux can be written as [19]

$$\vec{g}_k = \frac{n^2}{\rho}\sum_{j=1}^{\nu} m_j D_{kj}^a\left[\vec{\nabla}x_j + \left(x_j - \frac{\rho_j}{\rho}\right)\vec{\nabla}\ln p\right] - \frac{D_k^{Ta}}{m_k}\vec{\nabla}\ln T_k. \tag{8}$$

Here n is the total number density, x_j is the mole fraction of species j, ν is the number of different species, ρ_j is the mass density of species j, m_k is mass of species k, p is pressure, k_B is Boltzmann constant and T_k is the temperature of species k. D_{ij}^a is the general ambipolar binary diffusion coefficient between species i and species j and is related with the binary diffusion coefficient between the particles defined as [28]

$$D_{ij}^b = \frac{3k_B^2 T_i T_j}{16pm_{ij}^*\Omega_{ij}^{(1,1)}(T_{ij}^*)} \tag{9}$$

Here, T_i and T_j are temperatures of ith and jth particle respectively, $\Omega_{ij}^{(1,1)}$ is the collision integral and k_B is the Boltzmann constant. The reduced mass m_{ij}^* and reduced temperature T_{ij}^* are defined as follows:

$$m_{ij}^{*} = \frac{m_i m_j}{(m_i + m_j)}, \quad T_{ij}^{*} = \frac{m_i T_j + m_j T_i}{(m_i + m_j)}. \tag{10}$$

The first approximation to the general diffusion coefficients in terms of binary diffusion coefficients may be written as [29]

$$D_{ij} = \frac{F^{ji} - F^{ii}}{m_j |F|}, \tag{11}$$

where, F^{ij} is a cofactor of F_{ij}, defined in terms of binary diffusion coefficients as [29]

$$F_{ij} = \frac{1}{\rho}\left[\frac{n_i}{D_{ij}^{b}} + \sum_{l \neq i} \frac{n_l m_j}{m_i D_{il}^{b}}\right](1 - \delta_{ij}). \tag{12}$$

ρ, δ_{ij}, and n_i correspond to mass density, Kronecker delta symbol, and number density of species i. General, ambipolar diffusion coefficients are defined in terms of general diffusion coefficients as follows [19]:

$$D_{ij}^{a} = D_{ij} + \frac{\alpha_i}{\beta} \sum_k Z_k D_{kj}, \tag{13}$$

$$D_i^{Ta} = D_i^{T} + \frac{m_i \alpha_i}{\beta} \sum_k Z_k \frac{D_k^{T}}{m_k}, \tag{14}$$

where α and β can be expressed in terms of charge, mass, number density, temperature, and associated general diffusion coefficients of the participating particles as follows:

$$\alpha_i = \sum_j \frac{m_j n_j Z_j D_{ij}}{T_j}, \tag{15}$$

$$\beta = -\sum_i Z_i \sum_j \frac{m_j n_j Z_j D_{ij}}{T_j}. \tag{16}$$

Z_j refer to the number of charges of species j.

It is the diffusion process, described by Eqs. (7)–(16), which is solely responsible for the effect of demixing. From the equation itself, it is obvious that variation of the mole fraction gradient, thermal gradient, action of external forces like electric field [19] and collisional contributions may cause variation in the diffusion rates, resulting in the demixing process. The temperature gradient can give rise to the mole fraction gradient of individual species. In a mixture of two gases, a difference in the ionization potentials causes one gas to be more completely ionized at a given temperature, resulting in an increase in the total mole fraction of one of the gases. Here gas refers to all species derived from that gas (electrons, ions, atoms, and molecules). This leads to increased diffusion of the gas with the lower ionization potential to the regions at temperatures below the ionization temperature, resulting in demixing. A similar effect occurs when one of the gases is diatomic. Dissociation of the diatomic gas increases the mole fraction of that gas, causing it to diffuse into the regions at temperatures below the dissociation temperature. Another important cause for demixing is the existence of different frictional forces arising out of unequal collision cross sections among a pair of species. Unbalanced frictional forces lead to the demixing and they are found to be the most dominant process for such effects [20], particularly when there is a large difference between the masses of the gases.

III. A QUALITATIVE TREND OF THE RADIAL DEMIXING BEHAVIOR IN AN ARGON-HYDROGEN ARC USING A ONE-DIMENSIONAL 2-T MODEL

The nature of demixing differs widely with variation in gases. In this section a possible trend of radial demixing of argon and hydrogen is estimated for an SG-100 torch in which the experimental studies are performed. It is first necessary to know the distribution of the electron and the heavy particle temperatures inside the core. While some experimental profiles are used in [22] for the free burning arc, no experimental data are available for the electron and the heavy particle temperatures inside a nozzle. An accurate estimate of heavy particle and electron temperature distributions through rigorous fully nonequilibrium kinetic calculations including demixing effects requires involved computations which is currently a subject of another study. In this section we are interested only in the qualitative trend and use a one-dimensional model [23] to get some realistic distribution of the electron and the heavy particle temperatures inside the nozzle.

We consider the cylindrical nozzle section (diameter ~8 mm) of a SG-100 spray torch (details in Sec. IV) and assume that zero radial electric field and zero radial pressure gradient exist inside the nozzle. The gas pressure is 1 atmosphere and the nozzle wall stays at a temperature around 600 K. Inside the plasma column, all the electrons stay in equilibrium with each other at a temperature T_e which is different from T_h, the temperature followed by the rest of the particles inside the plasma. The two temperature Elenbaas-Heller equations [23] are solved iteratively with the boundary condition that the radial gradient of the electron temperature vanishes both at the wall and at the central axis and that of the heavy particle temperature vanishes only at the central axis. At the wall the temperature of the heavy particles reaches that of the wall. The plasma gas, employed in the study, is mainly argon mixed with a small fraction of hydrogen (<0.5% by mass in all cases). In estimating the approximate temperature profiles, two-temperature transport properties of argon alone have been considered. Here, it should be pointed out that depending on the degree of demixing, concentration of hydrogen near the wall might change significantly, thereby influencing the temperature profile near the edge. For example, a higher thermal conductivity of hydrogen may result in a sharper drop of temperature at the edge, enhancing the demixing further. For diffusion of argon into hydrogen, individual mole fractions have been properly considered in evaluating the associated diffusion coefficients. The exercise for arc currents of 300 A and 500 A results in the electron and the heavy particle temperature profiles as shown in Figs. 4(a) and 4(b), respectively.

For such an arc column, neglecting the diffusion due to a gradient in the total pressure and due to the external forces [19], the diffusion flux of species i can be written as [19]

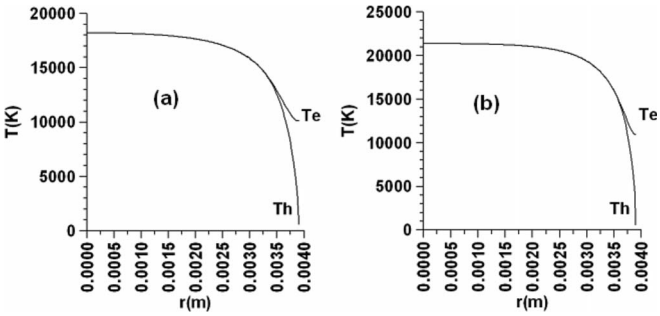

FIG. 4. Radial distribution of electron and heavy particle temperature inside the argon arc column at the nozzle (a) 300 A and (b) 500 A as obtained from the one-dimensional model.

$$\vec{g}_i = n_i \vec{v}_i = \frac{n^2}{\rho} \sum_{j=1}^{\nu} m_j D_{ij}^a \vec{\nabla} x_j - \frac{D_i^{Ta}}{m_i} \vec{\nabla} \ln T_i. \tag{17}$$

v_i is the diffusion velocity of the ith species relative to the mass average velocity.

For a mixture of two gases A (argon) and H (hydrogen), Murphy [17] has shown that it is possible to describe diffusion of one gas into the other using just one combined ordinary diffusion coefficient and one combined thermal diffusion coefficient. For a two-temperature plasma the number flux of gas A can be expressed as [24]

$$\overline{g_A} = \frac{n^2}{\rho} \overline{m_H} \, \overline{D_{AH}^x} \vec{\nabla} \overline{x_H} - \frac{\overline{D_{AH}^T}}{\overline{m_A}} \vec{\nabla} \ln T_h, \tag{18}$$

where $\overline{m_H}$ is the average mass of the heavy species of gas H; $\overline{D_{AH}^x}$ and $\overline{D_{AH}^T}$ are respectively combined ordinary and combined thermal diffusion coefficients.

$$\overline{g_A} = \sum_i s_i g_i, \tag{19}$$

where s_i's are stoichiometric coefficients.

Diffusion due to gradients in the nonequilibrium parameter (T_e/T_h), due to gradients in the total pressure and due to external forces [19] are neglected in Eq. (18). If the convection contribution is also neglected, the equilibrium mole fraction distribution of the gases can be calculated from the above equation setting $\overline{g_A}=0$. This leads to

$$\vec{\nabla} x_H = -\vec{\nabla} x_A = \frac{\rho}{n^2} \frac{\overline{D_{AH}^T} \vec{\nabla} \ln T_h}{\overline{m_A} \, \overline{m_H} \, \overline{D_{AH}^x}}. \tag{20}$$

This equation can be integrated with appropriate boundary conditions to obtain the distribution of mole fractions in radial direction. As can be noted from the study of Rat *et al.* [24], both the ordinary and thermal diffusion coefficients depend heavily on the actual mole fraction as well as on the temperature nonequilibrium parameter $\theta(=T_e/T_h)$. Once diffusion induces a change in the mole fraction at a certain location, the composition of the plasma changes and so do

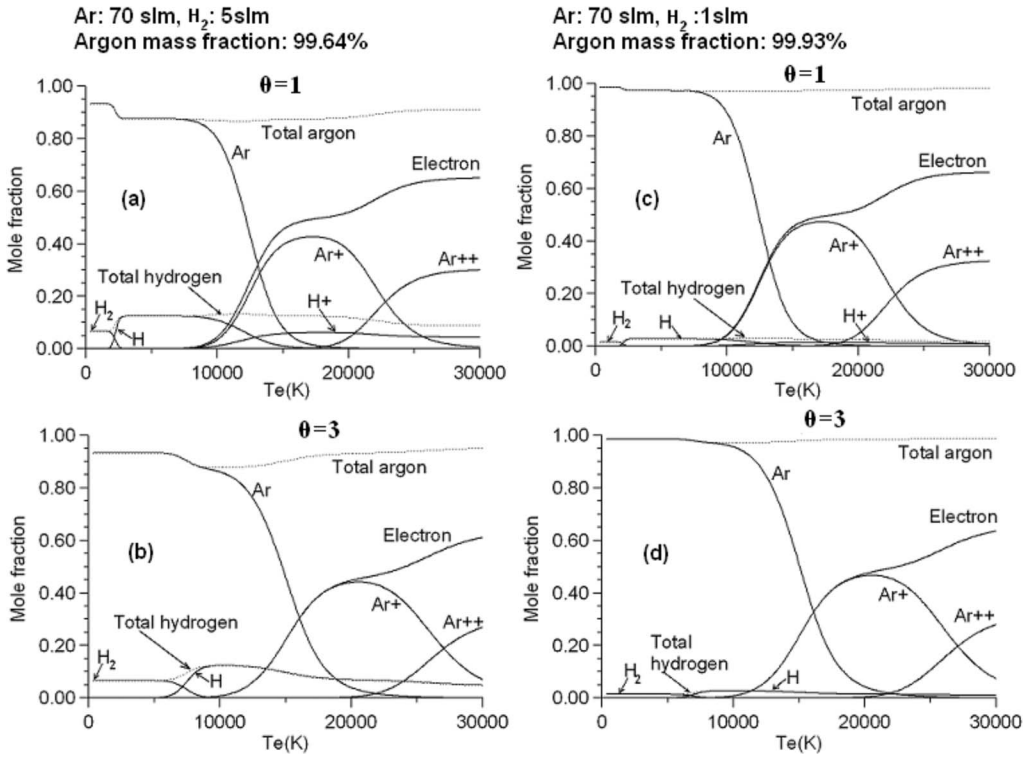

FIG. 5. Mole fraction variation with electron temperature for different $\theta(=T_e/T_h)$ values: (a),(b) Ar: 70 slm; H_2: 5 slm; (c),(d) Ar: 70 slm; H_2: 1 slm.

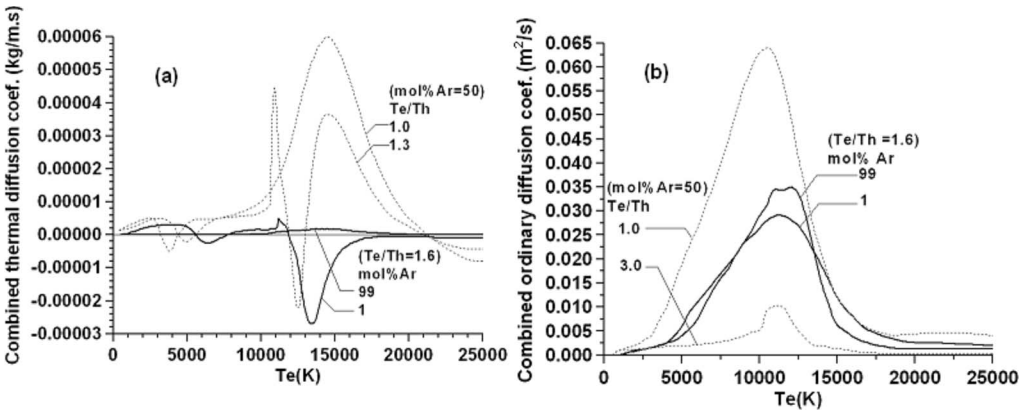

FIG. 6. Typical strong dependence of (a) combined thermal diffusion coefficient and (b) combined ordinary diffusion coefficient with mole fraction and temperature nonequilibrium (T_e/T_h).

the values of the associated diffusion coefficients and the number densities at that location. Therefore, the solution of the above equation is obtained self-consistently in an iterative manner so that after sufficient iterations the change in the mole fraction distribution at every location in consecutive iterations becomes insignificant and the final distribution is reached.

While the diffusion coefficients, identical to those in Ref. [24], have been used in the simulation, for a given x_H, T_e, and θ, the composition of an argon-hydrogen plasma is derived from the two-temperature Saha equation [30] and from these data the average mass density, $\rho(r)$, is computed. Obtained variations in the mole fraction with temperature for different species are shown in Fig. 5 for different nonequilibrium parameters $\theta(=T_e/T_h)$ and mass fractions. The typical strong dependence of the combined thermal diffusion coefficient on mole fraction and θ is presented in Fig. 6. The variation is rather strong in the region of higher temperatures and even leads to a change in the sign of the combined thermal diffusion coefficient, depending on the condition. It is evident from Eq. (20) that even if the temperature remains the same, an appropriate change in the mole fraction value or a change in θ alone can lead to a decrease in the mole fraction with temperature instead of an increase. Therefore, the results obtained for equilibrium conditions [19,20] may deviate significantly in the case of temperature non-equilibrium and the resulting mole fraction variations must be taken into account.

For boundary condition of x_H, a zero radial gradient is assumed along the symmetry axis ($r=0$) and the boundary condition at the wall is derived from mass conservation:

$$\int_{r=0}^{R} 2\pi\rho_H(r)v(r)dr = M_H, \tag{21}$$

where M_H is the total mass flow rate of hydrogen (a known parameter from inlet conditions) and R is the radius of the channel. The used velocity profiles $[v(r)]$ in the computation are shown in Fig. 7. The profiles are only approximate and profile parameters are chosen realistically from velocity measurement results of [31]. It should be mentioned here that for a given current, a fixed temperature profile as derived in the previous section and a fixed velocity profile as in Fig. 7 is used in the computation. For the range of hydrogen mass fractions considered in the manuscript (less than about 0.006), the results given in Table 1 of Ref. [20] indicate that the temperature profile is only weakly dependent ($<3\%$) on the hydrogen mass fraction, although there is a significant ($\sim 25\%$) increase in the flow velocity when hydrogen is added to pure argon at a mass fraction of 0.005. This suggests that it may be reasonable to choose the same temperature profile for different Ar/H mixtures. However, considering radial variation of the composition through demixing and approximate velocity profiles, obtained results can only describe qualitative trends of the possible behavior.

The mole fraction distributions of hydrogen in radial direction as obtained from the solution of the above equations are displayed in Fig. 8 for arc currents of 300 A and 500 A. Since θ tends to be more than 3, the solution in the immediate vicinity of the wall is not reliable (due to lack of available diffusion coefficient data for $\theta > 3$), and is not presented in the figure. To explain the specific trend of the observed behavior it may be noted from Eq. (20) that the hydrogen mole fraction gradient (x_H) depends on the magnitude and the sign of $\overline{D_{AH}^T}$ (combined thermal diffusion coefficient), $\overline{D_{AH}^x}$ (combined ordinary diffusion coefficient), and $\vec{\nabla} \ln T_h$ (temperature gradient of heavy particles). $\overline{D_{AH}^T}$ and $\overline{D_{AH}^x}$ in turn, depend on mole fraction, temperature, and the temperature nonequilibrium parameter θ (Fig. 6). Since $\overline{D_{AH}^x}$ is always positive and $\vec{\nabla} \ln T_h$ is always negative, an increase or

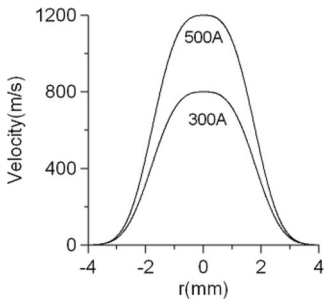

FIG. 7. Velocity profiles used in the study for $I=300$ A and $I=500$ A.

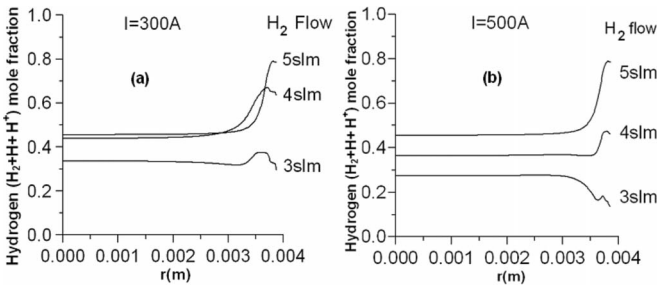

FIG. 8. Distribution of hydrogen mole fraction in radial direction as obtained from solution of the demixing equation for arc current: (a) 300 A; (b) 500 A.

decrease in x_H with radius is ultimately determined by the sign of $\overline{D_{AH}^T}$. For T_h less than 3000 K, $\overline{D_{AH}^T}$ is always positive for any θ and any mole fraction [24]. As a consequence an increase in x_H is observed with a decrease in the radius near the edge. Since T_H increases very fast with a decrease in the radius (Fig. 4), this region is very narrow and as T_h increases $\overline{D_{AH}^T}$ will be negative in some region between 3000 and 7000 K (depending on the mole fraction and θ) [24]. This region then starts exhibiting a decrease in x_H with decrease in radius. Since this region also meets the very steep radial gradient in T_H (Fig. 4), the associated decrease in x_H with radius is very sharp. For further decrease in radius, the temperature increases and $\overline{D_{AH}^T}$ again becomes positive; x_H starts to increase again with a decrease in radius. However, this approaches the region near the central axis of the nozzle for which the factor $\vec{\nabla} \ln T_h$ [Eq. (20)] itself tends to vanish (Fig. 4), and therefore results in a small increase in x_H with a decrease in r. However, beyond around 20 000 K, $\overline{D_{AH}^T}$ always becomes negative for all θ and any mole fraction [23], i.e., one can expect a decrease in x_H with a decrease in r even near the center of the arc in such cases (if $\vec{\nabla} \ln T_h$ is still significant and such a temperature zone exists there).

While the scenarios are different for different currents and mass flow rates, it is seen (Fig. 8) that for a given current it is the boundary layer that is the most affected zone by the change of the hydrogen flow. For example, at 300 A, the hydrogen mole fraction changes from nearly 0.8 to 0.3 as the hydrogen flow changes from 5 slm to 3 slm. It is obvious from the results [Fig. 8(a)] that it may be possible to influence the boundary layer alone, without significantly affecting the core region. Appropriate fluid dynamic simulation (2D simulation is the minimum requirement to get the velocity profiles) and property calculation routines can accurately estimate the associated changes in the thermophysical properties of the boundary layer with a change in the inlet conditions. A study of corresponding changes in the experimental instability features may then reveal the details of the dynamics.

TABLE I. Operating regime of the experiment.

Quantity	Lower limit	Upper limit	Incremental steps
Ar flow	42 slm	70 slm	7 slm
H_2 flow	1 slm	5 slm	1 slm
Arc current	300 A	700 A	200 A

IV. EXPERIMENTAL SYSTEM

The experiments have been performed with an industrial plasma spray system built by Praxair [32]. A schematic of the electrical connections and gas flow control are shown in Fig. 9(a). Details of the water cooled plasma torch SG-100, used for the instability study, is shown in Fig. 9(b). SG-100 bears the basic features similar to most of the common thermal plasma torches and has a nozzle bore of diameter 7.8 mm. A constant current, regulated power supply PS100 is used for sustained operation, and a high frequency starter unit, HF200, is used for ignition of the arc. The flow control console 3610 (using method of critical orifices to measure gas flow rates) is used for argon and a separate mass flow controller, Sierra 810C (range 0–5 slm of H_2), is used for controlling the hydrogen flow. The gases after passing through a check-valve, enter a quarter inch tee to get mixed and then the gas mixture enters the plasma torch through a custom made 12-hole straight gas injector. Experiments have been performed for different settings of the individual gas flow rates and different currents as shown in the operating regime chart in Table I. The voltage evolution across the arc [Fig. 9(a)] for each setting has been sampled at intervals of 10 ms and stored using a four channel oscilloscope HP54540A for subsequent analyses.

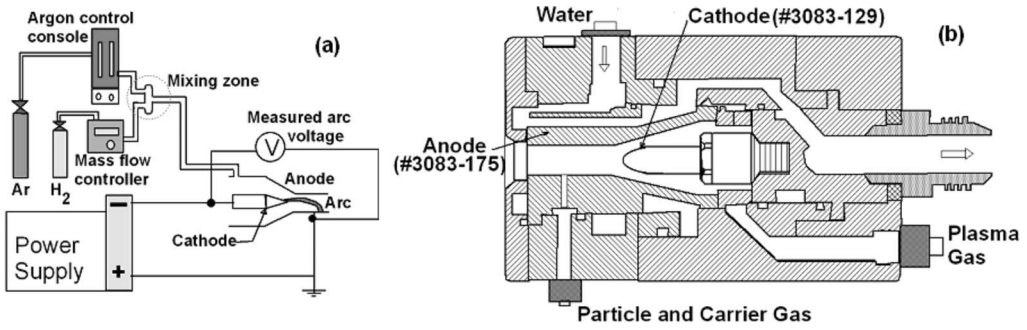

FIG. 9. Schematic of (a) the electrical connections and flow control and (b) the plasma torch Praxair-SG100, used in the instability study using binary gas mixtures.

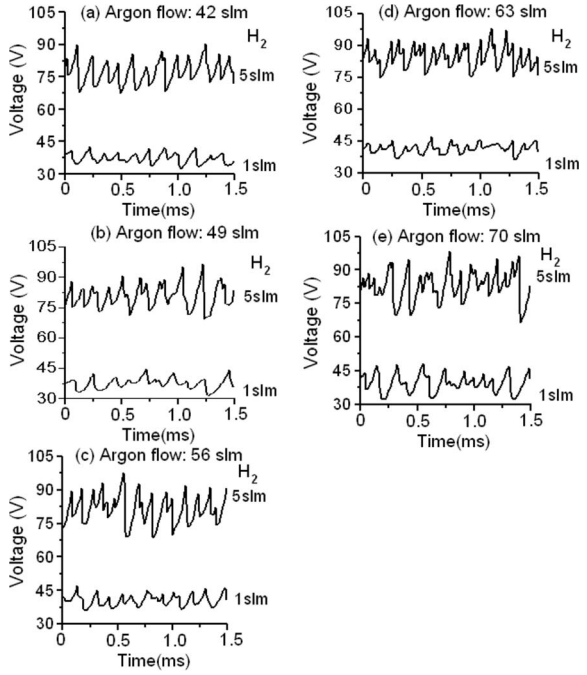

FIG. 10. Variation of instability features with argon flows: (a) 42 slm, (b) 49 slm, (c) 56 slm, (d) 63 slm, and (e) 70 slm. Fluctuations of arc voltages are presented for 1 slm and 5 slm of hydrogen in each figure. Arc current =500 A. A DC shift of 30 V is applied to the signals with 5 slm of H_2.

V. RESULTS AND ANALYSES

A. Identifying instability originating zones

Figure 10 shows the instability features as reflected in measured arc voltage traces for the arc current of 500 A. Argon flow varies from 42 slm to 70 slm in steps of 7 slm as one moves from Fig. 10(a)–10(e). In each figure, for a given argon flow two instability features are presented: One for hydrogen flow of 5 slm and the other for hydrogen flow of 1 slm. While a gradual transition is observed with increase in hydrogen flow rate, it is observed that, at any argon flow rate, a change of hydrogen flow by as little as 4 slm causes significant visible changes in the instability features in each of these figures. Interestingly, there is almost no apparent change in the instability features as one changes the argon flow by as much as 21 slm [Fig. 10(a)–10(d)]. Appreciable change in amplitude is noticed for the lower traces (1 slm) as one moves from Fig. 10(d) to Fig. 10(e). A possible explanation is that due to the demixing effect, a change in inlet argon flow influences the argon concentration in the core rather than the boundary layer which is primarily dominated by hydrogen. Since, the instability originates from the boundary layer, the feature of the instability remains unchanged. On the other hand, a little change of hydrogen flow immediately causes a change in the hydrogen concentration in the boundary layer due to the same effect. Consequently, a significant change in the instability feature occurs. However, if the argon flow is changed drastically, associated changes in the core flow may be strong enough to influence the boundary layer also. In that case a change in the instability features may be observed from a change in the argon flow. Such a change is observed in Fig. 10(e) after an increase of 28 slm of argon flow compared to Fig. 10(a).

The associated behavior of the instability in frequency space under the mentioned variations in the flow rates of the component gases (Fig. 10) is presented in Fig. 11. It is observed that neither a change in the argon flow nor a change in the hydrogen flow influences the positions of the frequency

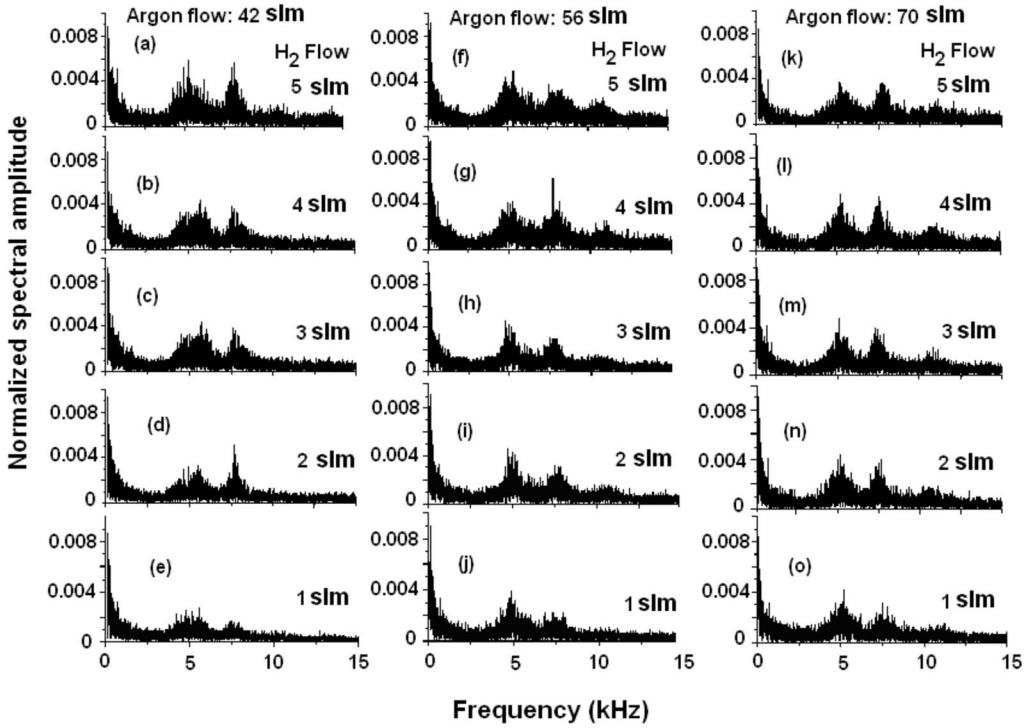

FIG. 11. Behavior of the instabilities in frequency space for different argon and hydrogen flow rates at an arc current of 500 A.

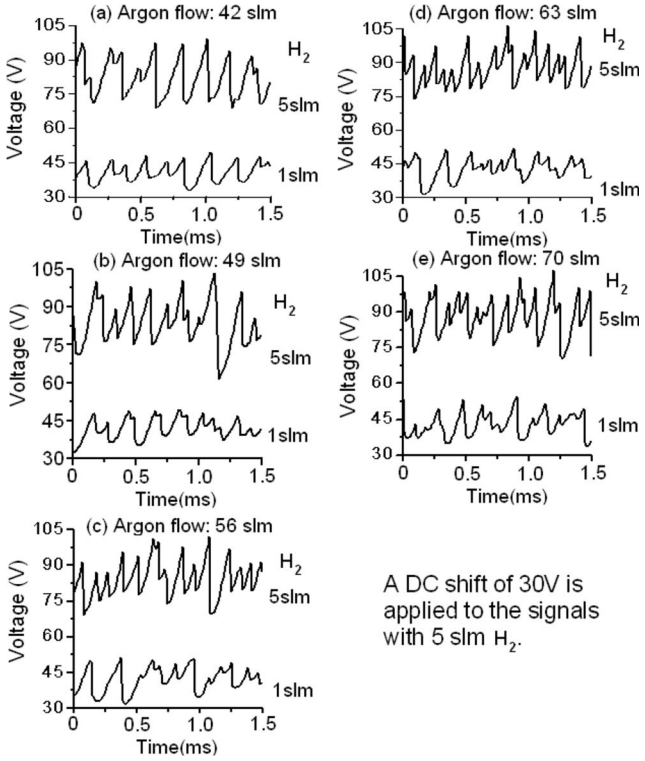

FIG. 12. Variation of instability features with argon flows: (a) 42 slm, (b) 49 slm, (c) 56 slm, (d) 63 slm, and (e) 70 slm. Fluctuations of arc voltages are presented for 1 slm and 5 slm of hydrogen in each figure. Arc current =300 A.

peaks, suspecting that although amplitudes of the instability do depend on the composition of the instability layer, frequencies have very weak dependence on it. Similar studies for lower (300 A) and higher (700 A) currents are presented in the following.

For 300 A [Figs. 12(a)–12(e)], the instability features remain almost unchanged even for a change of 28 slm of argon flow. However, for a given argon flow, a small change in the hydrogen flow significantly influences the instability features similar to that observed at 500 A. Again we see (Fig. 13) that the associated behavior of the instability in frequency space remains mostly unaltered for all conditions. However, when compared with the spectra of Fig. 11 (500 A), significant changes in the instability behavior in the frequency space may be detected. This leads to another important conclusion that the behavior of the instability in frequency space has a strong dependence on arc current.

At 700 A, because of higher temperature and a higher heat load at the anode arc root, some erosion of the anode takes place. Anode surface conditions change appreciably after some time of operation. While the results presented in Figs. 10–13 were reproducible even after a year with the same anode, results presented in Fig. 14 for 700 A were reproducible only within very short time intervals (~1 h). For lower flow rates of hydrogen, the arc was found to be steady showing almost no fluctuation. A trend of this can be seen in Figs. 14(a) and 14(b) for 3 slm of hydrogen. To avoid possible puncturing of the anode, experimentations under such conditions were discontinued.

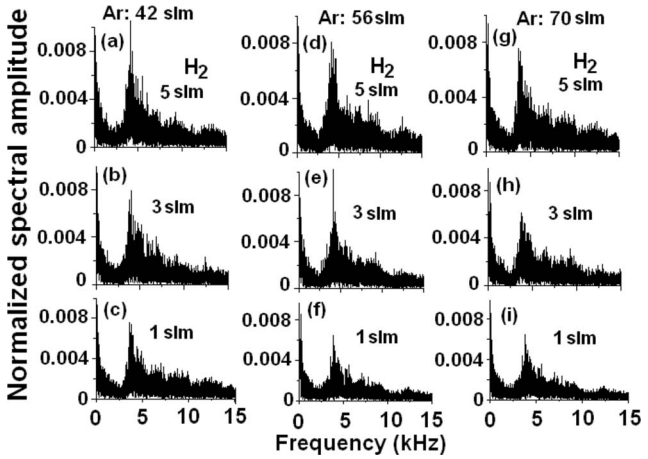

FIG. 13. Behavior of the instabilities in frequency space for different argon and hydrogen flow rates at an arc current of 300 A.

Similar to observations at 500 A and 300 A (Fig. 10 and Fig. 12), the instability features are not dependent on argon flow rate up to some extent (Fig. 14) and positions of the primary components of the dynamics on the frequency axis remain mostly unaltered (Fig. 15). However, an important fact may be noticed. For 300 A, even a change by 28 slm of argon was not able to change the instability features. For 500 A, a change of 28 slm of argon flow could make a visible change in the behavior. For 700 A, even a lower amount

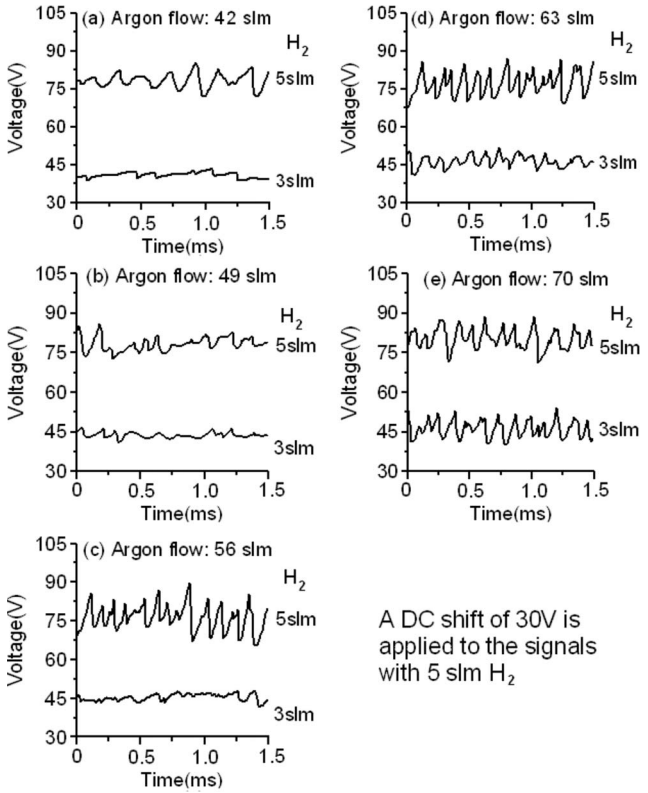

FIG. 14. Variation of instability features with argon flows: (a) 42 slm, (b) 49 slm, (c) 56 slm, (d) 63 slm, and (e) 70 slm. Fluctuations of arc voltages are presented for 3 slm and 5 slm of hydrogen in each figure. Arc current =700 A.

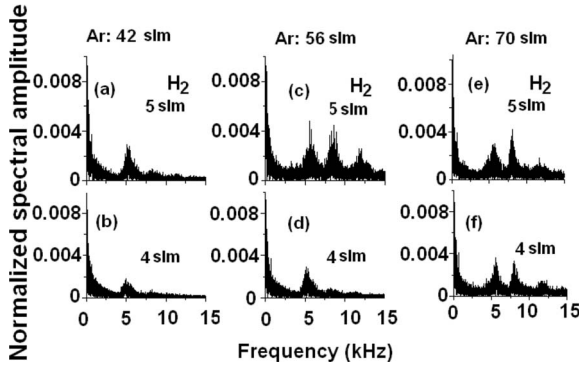

FIG. 15. Behavior of the instabilities in frequency space for different argon and hydrogen flow rates at an arc current of 700 A.

of argon flow (14 slm) is able to make a visible change. The observation leads to another important conclusion, i.e., the higher the arc current, the higher the mixing of the core gas with the gas in the boundary layer. Stronger electromagnetic body forces at higher currents have the capability of suppressing the underlying instability. Absence of the characteristic peaks in the spectra of Figs. 14(a), 14(b), and 14(d) corresponds to this. However, a small appearance of the characteristic frequencies can be also noticed even in these spectra.

From this study, it is now apparent that the instability originates from the boundary layer near the anode wall and the components of the observed dynamics in frequency space are controlled by the arc current. Since it is only the arc root region in the boundary layer through which the arc current passes, it appears that the instability originates from the region at and near the arc root.

The importance of the demixing process in the present study can be better understood from the mass ratio chart of Fig. 16. All of the operating points A, B, and C in Fig. 16 correspond to identical $Ar:H_2$ mass ratios in the uniformly mixed gas. But individual $Ar:H_2$ flow rates for the points A, B and C vary and they are respectively (42 slm:3 slm), (57 slm:4 slm), and (70 slm:5 slm). Therefore, without demixing there should be no change in the instability features as one shifts from one operating point to another (since mass ratio in the uniformly mixed gas does not change). At most, one can expect a change in the average arc voltage due to different flow velocities associated with different conditions A, B, and C. However, if demixing is active, individual mass flow rates are important rather than the mass ratio in the

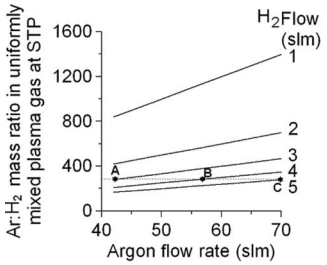

FIG. 16. Argon hydrogen mass ratios in flow space of argon and hydrogen at standard temperature and pressure (STP).

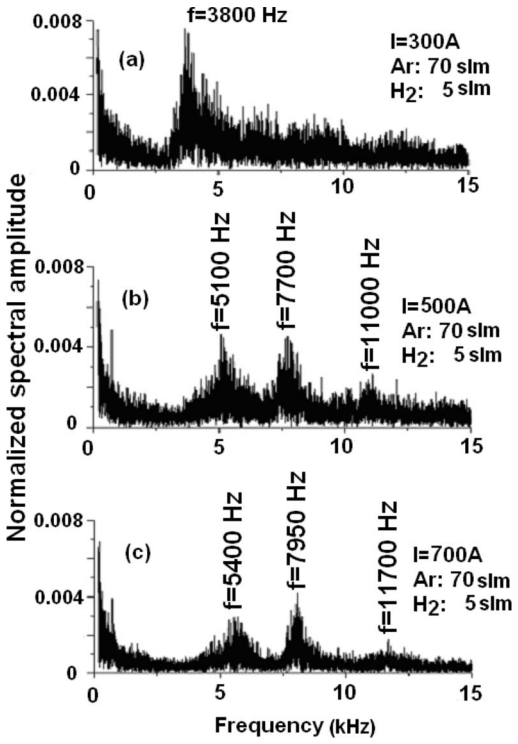

FIG. 17. Bifurcating behavior with change in arc current.

uniformly mixed gas and different instability features are expected in each case. This is indeed the feature exhibited in all the experimental results presented. For example, the lower curve in Fig. 14(a) corresponds to point A and the upper curve in Fig. 14(e) corresponds to point C. Respective instability amplitudes are distinctly different. For low arc currents (~300 A), a thicker boundary layer exists over the anode and this seems to be the only explanation for the observed behavior. However, for higher currents, higher flow rates may influence the relatively thin boundary layer and may show its effect on the observed instability.

B. Changing frequency behavior with arc current

As observed in the previous section a variation in arc current causes change in the behavior of the dynamics in frequency space. Figure 17 presents such changes in behavior in some more detail. Approximate values of the major components are plotted in Fig. 18. As the current increases

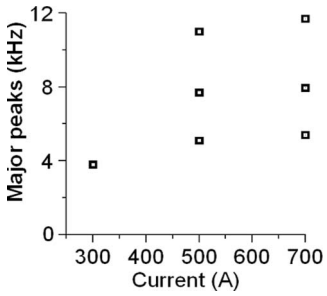

FIG. 18. Explicit variation of the primary frequencies.

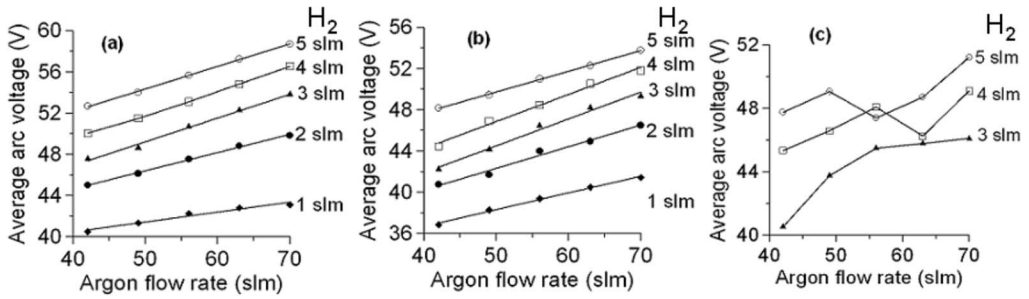

FIG. 19. Behavior of average arc voltage with varying flow of argon and hydrogen. (a) Arc current =300 A; (b) arc current =500 A; (c) arc current =700 A.

from 300 A to 500 A, the number of primary components of the dynamics changes from one to three. While a study with smaller current steps needs to be performed to allow the dependence on current to be better resolved, it can be concluded from the available data that, with increase in current, the dominant frequencies of the dynamics have a tendency to increase in number and to move towards higher frequency regimes. The frequency shift with increasing current becomes weaker at higher currents.

C. Effect of gas flow rates on average arc voltages at different currents

The instability amplitude depends on the plasma gas composition in the boundary layer and hence does not change with the change in the core flow. However, a major part of the arc path lies in the core itself. The arc path gets elongated more by the fluid dynamic drag force for higher flow rates of the core gas, resulting in a higher value of the average arc voltage. The instability-originated fluctuations are superimposed on this average arc voltage resulting in the actual values of measured arc voltages. Variation of arc voltages with core or boundary layer flow is almost linear for 300 A and 500 A [Figs. 19(a) and 19(b)]. However, for 700 A [Fig. 19(c)], the behavior is complicated. Rapid erosion of the anode at higher current is suspected to be the major cause for this. Localized high electric fields resulting from eroded surface morphology and possibly enhanced interactions between arc current and magnetic fields might be responsible for such behavior.

D. Quadratic zones of instability in flow space of binary gas mixtures at higher currents

It has been observed that enhanced electromagnetic body forces at higher currents are capable of suppressing the instability-originated dynamics. Increase in flow rates, sufficient to influence the composition of the boundary layer can overcome such actions and may be able to bring back the dynamics dominated by instabilities (see, for example, Fig. 14). Since demixing enhances hydrogen concentration in the boundary, it is expected that relatively smaller variations of the hydrogen will be effective for this and a relatively large variation of argon flow will be required to get similar effects. Figure 20 presents such observations for an arc current of 700 A. In a steady mode, the arc voltage exhibits fairly steady behavior. A major decrease in average arc voltages, significant reduction in acoustic noises and significant decrease in light emissions from the jet in steady modes make them distinctly different from the unsteady modes and easily identifiable. Higher flow rates produce sharp transitions from a steady to an unsteady mode. Therefore, the so-called takeover and restrike modes, both fall in the category of unsteady mode. Interestingly, the study exhibits the existence of a quadratic zone in flow space of a binary gas mixture where steady behavior is possible and beyond which the arc behaves unsteadily. Since, binary gas mixtures are in common use in various industrial applications, these results may be useful for further study.

VI. CONCLUSIONS

A mixture of hydrogen with primary plasma gas argon is used to investigate some fundamental aspects of arc instability exploiting the inherent demixing of binary gases in arcs. Using a two temperature one-dimensional model it has been shown qualitatively that owing to the inherent demixing process in arcs, the boundary layer and the core of the plasma column may be dominated by hydrogen and argon, respectively. While associated variations in instability features due to variation of argon flow reflect phenomena happening in the core, similar effects for variations in hydrogen flow reflect the phenomena happening in the boundary layer. In the

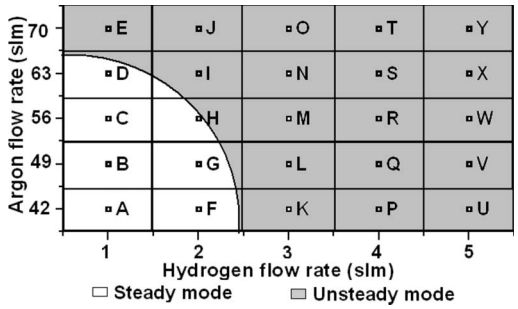

FIG. 20. Existence of quadratic zone in flow space of a binary gas mixture separating steady and unsteady behavior at 700 A for SG-100 torch. Separating boundary: $\alpha \cdot h^2 + (a-\beta)^2 = \gamma$; h: hydrogen flow (slm), a: argon flow (slm), $\alpha = 121$, $\beta = 38.5$, and $\gamma = 7.56 \times 10^2$. Operating points (A, B, C, D, F, G, H) exhibit steady behavior and other operating points (E, H, I–U) exhibit unsteady behavior in the experiment.

experiment, it has been observed that for given hydrogen flow and arc current, the basic instability features remain unaffected for a wide range of variation of argon flow; only the average arc voltage varies. On the other hand, a smaller increase in hydrogen flow significantly changes the instability features under similar conditions. Identical behaviors have been observed for all values of currents studied. While the behavior with 300 A and 500 A are found to be highly reproducible, experiment with 700 A are reproducible only within a short time interval, mainly due to high rates of anode erosion at higher currents. The overall observations suggest that the arc instabilities originate in the boundary layer over the anode surface. The frequencies of the instabilities are primarily controlled by the arc current and remain mostly unchanged for a change in flow rate of plasma gases. In other words, the instability originates from that region over the anode boundary layer which carries current. Therefore, the study provides evidence that the instability originates from the region at or near the anode arc root.

Variation of average arc voltage with core as well as boundary layer flow has been found to be mostly linear for arc currents of 300 A and 500 A. However, for 700 A, a more complex behavior has been observed. Localized electric field from eroded surface morphology, body forces resulting from enhanced interactions between arc current and magnetic field are suspected to be responsible for such behavior.

A study on bifurcation behavior of the instability in frequency space as a function of arc current revealed a tendency of the instability to shift toward higher frequencies for higher arc currents as well as generation of new components. Further investigations with finer current steps are required to explore the basic routes followed in the bifurcation. Higher arc currents tend to suppress the instabilities.

For higher currents, a quadratic region has been found in the flow space of argon and hydrogen, within which the arc exhibits a steady behavior and beyond which the arc becomes unsteady. Since binary gas mixtures are in common use in various industrial systems, these results may be of interest for further investigations.

ACKNOWLEDGMENTS

This work was supported in part by the NSF under Grant No. CTS-0317429. One of the authors (S.G.) is thankful to Department of Atomic Energy, India, for grant of leave. The authors thank Dr. A. B. Murphy for many useful discussions.

[1] H. Maeker, Ann. Phys. **18**, 441 (1956).
[2] J. K. Harvey, P. G. Simpkins, and A. D. Adcock, AIAA J. **1**, 714 (1963).
[3] S. A. Wutzke, E. Pfender, and E. R. G. Eckert, AIAA J. **5**, 707 (1967).
[4] S. A. Wutzke, E. Pfender, and E. R. G. Eckert, AIAA J. **6**, 1474 (1968).
[5] J. F. Coudert, M. P. Planche, and P. Fauchais, Plasma Chem. Plasma Process. **16**, 211S (1996).
[6] M. P. Collares and E. Pfender, IEEE Trans. Plasma Sci. **25**, 864 (1997).
[7] Z. Duan and J. Heberlein, J. Therm. Spray Technol. **11**, 44 (2002).
[8] J. L. Dorier, M. Gindrat, C. Hollenstein, A Salito, M. Loch, and G. Barbezat, IEEE Trans. Plasma Sci. **29**, 494 (2001).
[9] M. Vysohlid, M.S. thesis, University of Minnesota, 2003 (unpublished).
[10] S. Ghorui and A. K. Das, Phys. Rev. E **69**, 026408 (2004).
[11] S. Ghorui and A. K. Das, IEEE Trans. Plasma Sci. **32**, 296 (2004).
[12] S. Ghorui, S. N. Sahasrabudhe, P. S. S. Murty, and A. K. Das, IEEE Trans. Plasma Sci. **32**, 308 (2004).
[13] T. Iwao, P. Cronin, D. Bendix, and J. Heberlein, IEEE Trans. Plasma Sci. **33**, 1123 (2005).
[14] G. Yang, P. Cronin, J. V. Heberlein, and E. Pfender, J. Phys. D **39**, 2764 (2006).
[15] P. Lenard, Ann. Phys. **11**, 636 (1903).
[16] W. Frie, Z. Phys. **172**, 99 (1963).
[17] A. B. Murphy, Phys. Rev. E **48**, 3594 (1993).
[18] A. B. Murphy, Phys. Rev. Lett. **73**, 1797 (1994).
[19] A. B. Murphy, J. Phys. D **31**, 3383 (1998).
[20] A. B. Murphy, Phys. Rev. E **55**, 7473 (1997).
[21] A. B. Murphy and K. Hiraoka, J. Phys. D **33**, 2183 (2000).
[22] S. C. Snyder, A. B. Murphy, D. L. Hofeldt, and L. D. Reynolds, Phys. Rev. E **52**, 2999 (1995).
[23] T. K. Bose and R. V. Seeniraj, Plasma Phys. Controlled Fusion **26**, 1163 (1984).
[24] V. Rat, J. Aubreton, M. F. Elchinger, P. Fauchais, and A. B. Murphy, Phys. Rev. E **66**, 056407 (2002).
[25] J. M. Bauchire, J. J. Gonzalez, and A. Gleizes, Plasma Chem. Plasma Process. **17**, 409 (1997).
[26] C. Baudry, A. Vardelle, and G. Mariaux, High Tech. Plasma Process. **9**, 1 (2005).
[27] M. Mitchner and C. H. Kruger, *Partially Ionized Gases* (Wiley, New York, 1973).
[28] J. D. Ramshaw, J. Non-Equilib. Thermodyn. **18**, 121 (1993).
[29] J. O. Hirschfelder, C. F. Kurtis, and R. B. Bird, *Molecular Theory of Gases and Liquids*, 2nd ed. (Wiley, New York, 1964).
[30] M. C. M. van de Sanden, P. P. J. M. Schram, A. G. Peeters, J. A. M. van der Mullen, and G. M. W. Kroesen, Phys. Rev. A **40**, 5273 (1989).
[31] M. P. Planche, J. F. Coudert, and P. Fauchais, Plasma Chem. Plasma Process. **18**, 263 (1998).
[32] *Operator's Manual: Model SG-100 Plasma Spray Gun* (Miller Thermal Inc., 1991).